PERGAMON

International Journal of Heat and Mass Transfer 43 (2000) 3917–3924

International Journal of HEAT and MASS TRANSFER

www.elsevier.com/locate/ijhmt

Effective conductivity computation of a packed bed using constriction resistance and contact angle effects

W.W.M. Siu, S.H.-K. Lee*

Department of Mechanical Engineering, Hong Kong University of Science and Technology, Clear Water Bay, Kowloon, Hong Kong

Received 4 June 1999; received in revised form 4 February 2000

Abstract

Effective conductivity computation is a major component in the study of conduction within a porous medium, consisting of packed spheres. For packings with porosity lower than 0.47, previous studies typically model the packed bed as an arrangement of cylinders with connecting webs. Not only does such system deviate from the actual structure, but its usage also requires empirically determined parameters. An alternative method is herein presented, and is valid for packed beds of porosity below 0.5, and where the conductivity of the sphere is much larger than that of the surrounding matrix. The present method approximates the packed bed as packed sphere systems consisting of different unit cells, and then using the presently computed relations to obtain the effective thermal conductivity. The relations were derived from constriction resistance relations, accounting for the angles formed between the contacting spheres. The results show for the first time, the necessity of properly accounting for these contact angles. Accounting for the contact angle, the effective thermal conductivity was computed for seven packed beds with porosities ranging from 0.18 to 0.47. The results were in excellent agreement with previous experimental and numerical work. © 2000 Elsevier Science Ltd. All rights reserved.

1. Introduction

Effective conductivity computation is a major component in the study of conduction within a porous medium consisting of packed spheres. Examples of such medium include sintered-particle systems, and particle-filled insulation systems. As shown in Fig. 1(a), such medium is typically modeled as a simple cubic structure with interconnecting linkages [1–4]. As this structure has a minimum porosity, ϕ, limit of 0.4764, studies requiring a structure with a lower porosity must typically alter this spherical packing into a regular arrangement of cylinders with connecting webs [5–8]. As the resulting structure further deviates from the actual structure, artificial parameters such as the area and length of the connecting webs are necessarily determined empirically.

Indeed, the above method has produced accurate results, but it is also dependent on the availability of experimental data. Thus, the method becomes less useful for new packing structures, where the empirical parameters have not been determined. In addition, while this method is adequate for conduction analysis, the unrealistic configuration would complicate the coupling with convective and radiative analyses. Finally, a parallel heat flow is often assumed in computing the effective conductivity [5,9,10]. However, this assumption begins to break down as the conductivity of the solid and the

* Corresponding author. Tel.: +852-2358-7186; fax: +852-2358-1543.

E-mail address: shklee@ust.hk (S.H.-K. Lee).

0017-9310/00/$ - see front matter © 2000 Elsevier Science Ltd. All rights reserved.
PII: S0017-9310(00)00051-X

Nomenclature

k	thermal conductivity, W/m K
N	number (spheres, contact, etc.)
n	number within an unit cell (spheres)
q, Q	heat flux (W/m^2), heat (W)
r, θ, ϕ	variables in spherical coordinates
R	thermal constriction resistance, K/W
V	volume, m^3
x	ratio of the deformation at a contact to the sphere radius

Greek symbols

α	thermal diffusivity, m^2/s
β	angle between two contacts, rad
ϕ	porosity
γ	ratio of contact radius to sphere radius, r_c/r_s

Subscripts

a, A	spheres connected in parallel, and per unit cross-sectional area
b, c, o	bulk, contact and local
eff	effective
l, L	spheres connected in series, and per unit length
s	sphere, or length scale with r_s
t	thermal path

matrix component take on different magnitudes. That is, the computation may not be accurate if the conductivity of the solid component is much higher than that of the matrix component, such as in a sintering system or for packed beds in a vacuum environment.

The objective of this study is to develop another method that can be more flexible in calculating the effective thermal conductivity of such sphere-packing structures. Using an appropriate packing structure, such as simple cubic (SC), body-center cubic (BCC) or face-center cubic (FCC), and approximating the mean contact area, the effective thermal conductivity is directly computed. Thus, by retaining the sphere-packing structure shown in Fig. 1(b), this method can be easily extended to account for simultaneous convective and radiative effects. The present method relies on computing the proper constriction–resistance relations and the key lies in properly accounting for the contact angle between the contacting spheres. This is shown schematically in Fig. 2. Thus, this study complements an earlier work [11] on computing the transient behavior of packed beds in a 180° orientation.

In the present study, the resistances for varying contact angles are introduced and using these, the effective conductivity are computed for packed beds with porosity values ranging from 0.2 to about 0.5. The packed beds are approximated as the SC, BCC and FCC regular packing structures. These are shown schematically in Fig. 3. The results show the computed value of the effective conductivity to agree closely with experimental value and furthermore, the neglect of the above-mentioned contact angle would introduce a considerable error.

2. Analysis

2.1. Packing structure

Packed beds, consisting of a single homogeneous

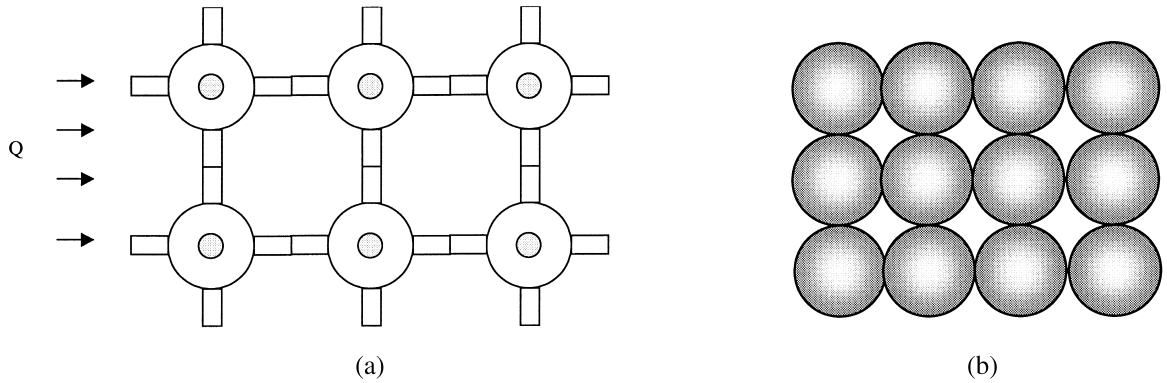

Fig. 1. Schematic of the structure used by (a) the previous studies and (b) present study.

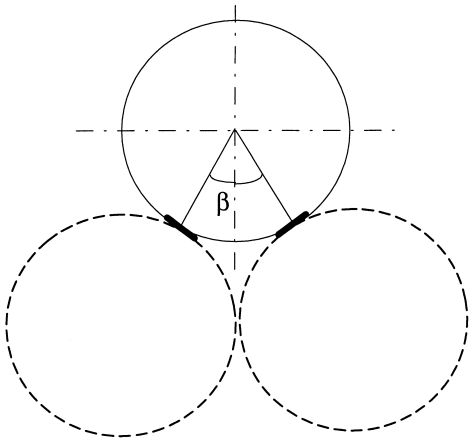

Fig. 2. Schematic showing the formation of the contact angle between three contacting spheres.

solid, typically have a porosity less than 0.5. For these, the packing can be closely approximated as arrangements of uniform-sized spheres. Thus, by using different arrangements, packed beds of different porosities can be obtained. Consistent with the findings from previous sintering studies [12,13], the present work utilizes the SC, the BCC and the FCC arrangements for different ranges of porosity values (Table 1).

These structures are shown schematically in Fig. 3, and from simple geometrical relations, the porosity for each of these structures can be computed by Eq. (1). The only unknown parameters in this equation are γ and x, which are, respectively, the contact radius ratio and sphere deformation ratios. Assuming the spheres to undergo elastic deformation, a unique relation exists between these two ratios [14], which is given in Table 2. Therefore, the porosity of these three packing structures can be uniquely determined, or vice versa, given a target porosity, a structure can be chosen according to Table 1, and the resulting value of γ and x can be determined; γ is a necessary parameter in calculating k_{eff}.

Table 1
Suitable packing arrangements for different porosity ranges

Simple cubic (SC), $N_c = 6$, $n_s = 1$, $V = 8r_s^3$	ϕ: 0.5–0.35
Body-center cubic (BCC), $N_c = 8$, $n_s = 2$, $V = 64r_s^3/(3\sqrt{3})$	ϕ: 0.3–0.25
Face-center cubic (FCC), $N_c = 12$, $n_s = 4$, $V = 32r_s^3/(\sqrt{2})$	ϕ: 0.2 and below

$$\phi = 1 - \left\{\frac{4}{3}\pi r_s^3 - N_c(r_s\gamma)^2 r_s x\right\} n_s/V \tag{1}$$

2.2. Effective thermal conductivity

$$Q = k_{\text{eff}} A\frac{\Delta T}{L} \Longrightarrow k_{\text{eff}} = \frac{L}{A}\frac{Q}{\Delta T} \tag{2}$$

The effective thermal conductivity of each unit cell of the packing structure can be computed from the Fourier's Law given in Eq. (2), where Q is the total heat flow resulting from the driving potential of ΔT. Invoking the definition of the thermal resistance, the effective conductivity can be equivalently expressed by Eq. (3), where L and A are the length and cross-sectional area of the unit cell, while R is the total resistance imposed by the unit cell.

$$k_{\text{eff}} = \frac{L}{A}\frac{1}{R} \tag{3}$$

For a unit cell where the conductivity of the sphere is much larger than that of the surrounding matrix, this total resistance is the sum of the resistances within and between the spheres. Assuming a system undergoing sintering, or under sufficiently high pressure, the

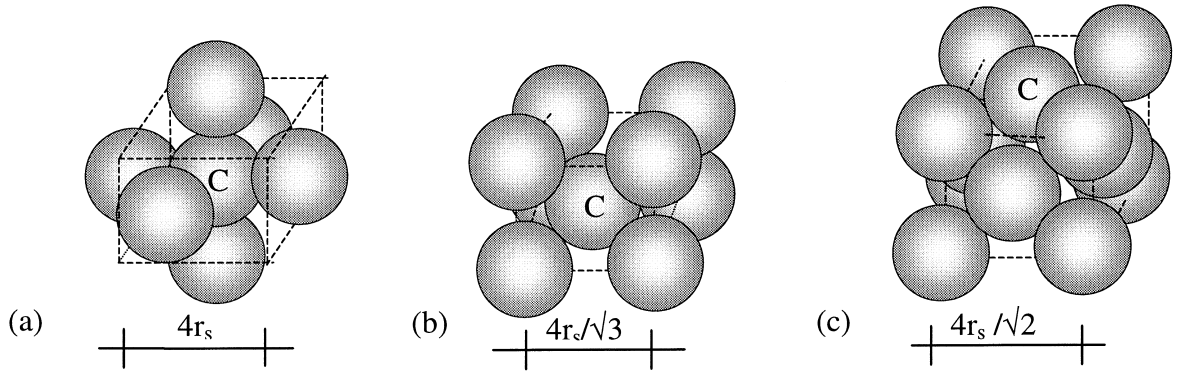

Fig. 3. Schematic of the (a) simple cubic, (b) body-center cubic and (c) face-center cubic unit cells.

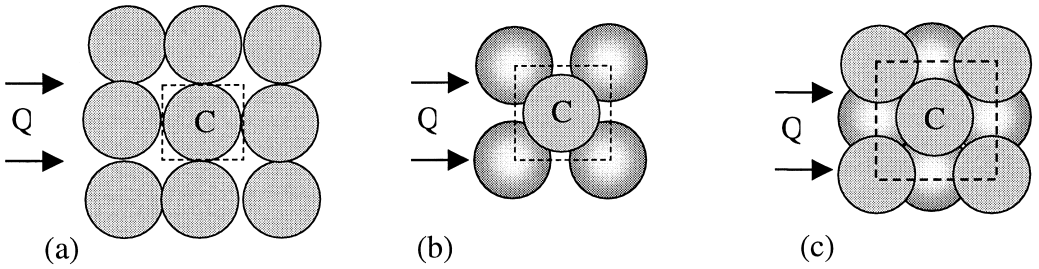

Fig. 4. Sectional view showing the thermal path through sphere "C" in the (a) simple cubic, (b) body-center cubic and (c) face-center cubic unit cells.

value of the contact resistance may be neglected. Thus, the total resistance, R, becomes dependent on the total thermal path, which is different for various packing structures.

Shown in Fig. 4 are the schematics of the SC, BCC and FCC unit cells, subjected to a uni-directional heat flow, Q, from the left to the right. In Fig. 4(a), the heat passes from the left sphere to the right sphere through sphere "C", and the resulting angle formed between these three spheres is 180°. Denoting these three contacting spheres as one thermal path, it is noted that sphere "C" in the SC unit cell contains only one thermal path of 180° orientation (Fig. 5(a)). In contrast, the BCC and FCC unit cells shown in Fig. 5(b) and (c) contain four parallel thermal paths through sphere "C", with respective orientations of 70.53° and 90°. Denoting $R(\beta)$, as the resistance of one thermal path with orientation of β, it is clear that for a SC unit cell, the resistance, R_s, imposed by sphere "C" is $R(180)$, and those imposed by sphere "C" in the BCC and FCC unit cells are $R(70.53)/4$ and $R(90)/4$, respectively. In general form, this is given below in Eq. (4), where for a packing of mono-size spheres, the contact angle, β, can vary from 180° to 60°.

$$R_s = \frac{R(\beta)}{N_t} \tag{4}$$

For a packed sphere system, every sphere except for those at the boundary is a sphere "C". Thus, R_s given in Eq. (4) is essentially the resistance of each interior sphere in the system, and for a packing with large number of spheres, the total thermal resistance of the packed bed is given by Eq. (5). In Eq. (5), N_a and N_l are, respectively, the number of spheres connected in parallel and series.

$$R = R_s \frac{N_l}{N_a} \tag{5}$$

$$k_{eff} = \frac{L}{A}\frac{N_a}{N_l}\frac{N_t}{R(\beta)} = \frac{N_A}{N_L}\frac{N_t}{R(\beta)} \tag{6}$$

Thus, the effective thermal conductivity can be determined by combining Eqs. (3) and (5), and introducing the parameters N_L and N_A, which, respectively, represent N_l per unit length and N_a per unit cross-sectional area. The final expression for the effective thermal conductivity is given above in Eq. (6), and the values of the parameters are summarized in Table 3. The only remaining unknown in Eq. (6) is $R(\beta)$, which represents the dependence of the constriction resistance on the contacting angles. As this is not available in the literature, it is computed within this study.

2.3. Constriction resistance

The key to obtaining the constriction resistance (hereafter simply referred to as the resistance) for varying contact angle is to recognize that it actually consists of two components, and only one of which is affected by the angle. As illustrated by the cylindrical object in Fig. 6 and expressed in Eq. (7), the resistance

Table 2
Relations between the contact radius and deformation ratios for spheres under elastic deformations

Contact radius ratio, γ	Deformation ratio, x
0.1	0.008
0.15	0.015
0.2	0.028
0.25	0.037
0.3	0.05

Table 3
Summary of parameters for different packing structures

	N_A	N_L	N_t	$R(\beta)$
Simple cubic, SC	$1/(4r_s^2)$	$1/(2r_s)$	1	$R(180°)$
Body-center cubic, BCC	$3/(16r_s^2)$	$\sqrt{3}/(2r_s)$	4	$R(70.53°)$
Face-center cubic, FCC	$1/(4r_s^2)$	$1/(\sqrt{2}r_s)$	4	$R(90°)$

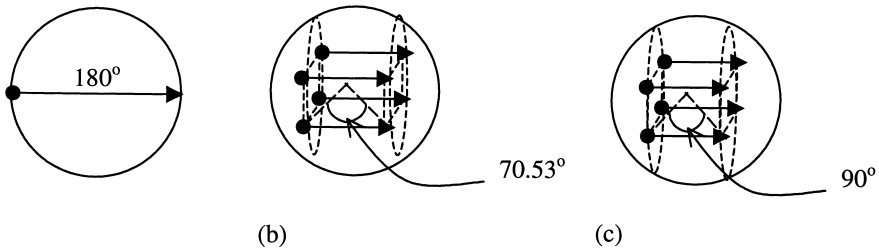

Fig. 5. Schematic showing the angle of the thermal path in the (a) simple cubic, (b) body-center cubic and (c) face-center cubic unit cells.

consists of a bulk resistance, R_b, and a local resistance, R_o. The former accounts for the distance separating the two areas across the cylinder and the latter accounts for the additional resistance caused by the presence of the constricted contact areas.

$$R = R_b + R_o \tag{7}$$

Thus, for the sphere shown in Fig. 7, the contact angle only affects the separation between the two contacts, and is thus expected to affect only the bulk resistance, R_b. On the other hand, the local resistance, R_o, is expected to be a function of the contact radius and independent of the contact angle, β. As a result, by subtracting the resistances at two different angle, the result would be proportional to the differences in the separation distance. This is given below in Eq. (8).

$$\left[R(180) - R(\beta)\right] \propto r_s(1 - \sin(\beta)/2) \tag{8}$$

Therefore, to determine the functional dependence of R on β, it would be sufficient to obtain R at only a few angles and then to use Eq. (8) as the basis of a correlation.

In order for $R(\beta)$ to be useful in Eq. (6), it must be computed for a sphere subject to heat flux conditions. To compute this resistance, the configuration in Fig. 7 is utilized, and the three-dimensional, steady-state temperature distribution inside a stainless steel-304 sphere is solved with equal and opposite heat flux conditions, of 5×10^9 W/m^2, imposed at the two contacts. Once the steady-state temperature is known, the constriction resistance is computed by dividing the difference between the two resulting contact temperatures by the imposed heat flow. To obtain the steady-state temperature, the sphere is initially assumed to be at 0°C, and the transient conduction equation, as given below in Eq. (9), is solved subject to the boundary conditions given in Eq. (10).

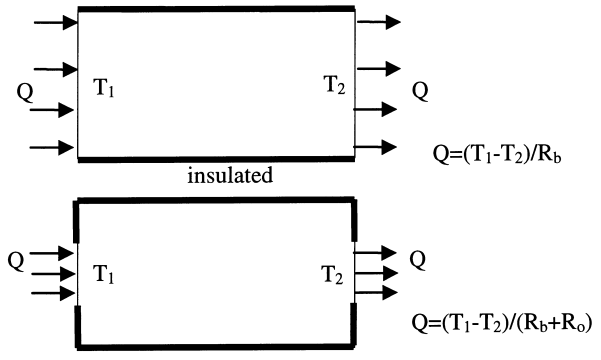

Fig. 6. Schematic illustrating the bulk and local constriction resistance of a cylinder.

$$\frac{\partial T}{\partial \tau} = \alpha\left[\frac{\partial^2 T}{\partial r^2} + \frac{2}{r}\frac{\partial T}{\partial r} + \frac{1}{r^2 \sin\theta}\frac{\partial}{\partial \theta}\left(\sin\theta \frac{\partial T}{\partial \theta}\right) + \frac{1}{r^2 \sin^2\theta}\frac{\partial^2 T}{\partial \phi^2}\right] \tag{9}$$

$$\begin{aligned} &r = r_s : (\beta - \theta_c)/2 < \theta < (\beta + \theta_c)/2 \quad \text{and} \\ &\quad 0 < \phi < \phi_c \\ &\quad -k\frac{\partial T}{\partial r} = q \\ &(\beta - \theta_c)/2 < \theta < (\beta + \theta_c)/2 \quad \text{and} \\ &\pi < \phi < (\pi + \phi_c) \\ &-k\frac{\partial T}{\partial r} = -q \\ &(\beta - \theta_c)/2 > \theta \quad \text{or} \quad \theta > (\beta + \theta_c)/2 \quad \text{or} \quad \phi_c < \phi < \pi \\ &\text{or} (\pi + \phi_c) < \phi < 2\pi \\ &-k\frac{\partial T}{\partial r} = 0 \end{aligned} \tag{10}$$

In the above equations, θ_c and ϕ_c are the angles subtending the square contact areas, which for comparison purposes can be converted into an equivalent contact radius given below in Eq. (11) [15,16].

$$r_c = (A_c/\pi)^{1/2} \tag{11}$$

Eq. (9) was solved using a finite volume formulation, and in order to increase the temperature resolution near the contact, the multi-spatial-temporal grid method [17] was employed. This method provides the

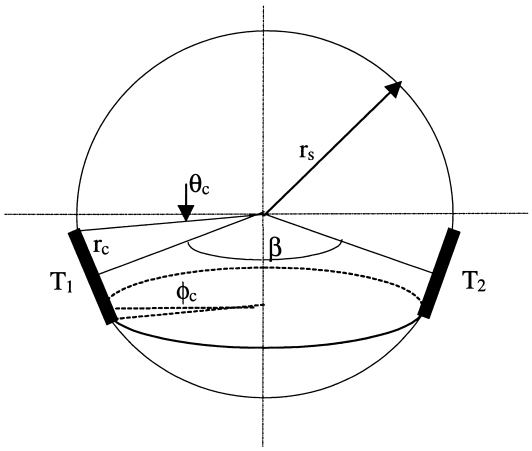

Fig. 7. Schematic of a sphere with two contacts at non-diametrical positions.

requisite spatial resolution without causing a tremendous increase in the computational time. In brief, this is accomplished by simultaneously implementing grid reduction and multiple timesteps. The resulting algebraic expressions were solved using Tri-Diagonal Matrix Algorithm (TDMA) and Crank–Nicolson scheme [18].

3. Results and discussion

3.1. Validation and resistance relations

The results were confirmed to be parameter independent. The model had previously been validated in two previous studies [11,17] and thus only some of the essential features of the validation will be repeated here. This consists of testing for physical consistency, and direct comparison with selected degenerate cases. The former consisted of verifying for trend consistency, and the latter consisted of comparing the steady-state resistance ($\beta = 180$) against those obtained by previous investigators [23,24], including the previous results generated by Siu and Lee [11] through a different model. The comparison shown in Fig. 8 indicates excellent agreement.

The resistance values were obtained for various sphere sizes, contact-radius ratios and contact angles, and these are shown in Fig. 9. As expected, the results collapsed onto one curve and consistent with previous discussions (Eq. (8)), they correlate to the function of $(\sin\beta/2)$. This correlation is also plotted on Fig. 9 and is given below by Eq. (12), where $R(180)$ was correlated in a previous study [11] and repeated here for completeness. This correlation is valid for the range between 60° and 180°, and despite the large degree of correlation, a minor discrepancy is noted near $(\sin\beta/2) = 0.5$, or when $\beta = 60°$. This discrepancy is due to the close proximity of the two contacts and the subsequent mutual influence. This is an issue for a later study.

$$R(\beta) = R(180) + \left[0.64\sin^2(\beta/2) - 0.08\sin(\beta/2) - 0.56\right] \times (kr_s) \tag{12}$$

$$R(180) = \frac{0.54038}{kr_s\gamma}\left[1 + 1.92069(\gamma) - 9.18530(\gamma^2) + 17.5257(\gamma^3)\right] \tag{13}$$

3.2. Effective thermal conductivity

Combining the above correlation with Eq. (6) allows for the computation of the effective conductivity for the SC, BCC and FCC unit cells as a function of the contact radius ratio, γ. As shown in Fig. 10, the conductivity for the FCC unit cell is greater than that for the BCC unit cell which in turn, is greater than that for the SC unit cell. More importantly, the dimension-

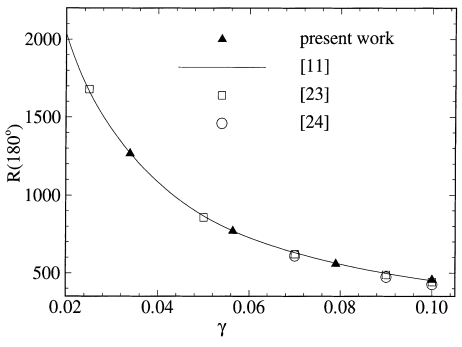

Fig. 8. Validation comparison of the presently computed steady-state resistance at $\beta = 180$ against those obtained by previous investigators.

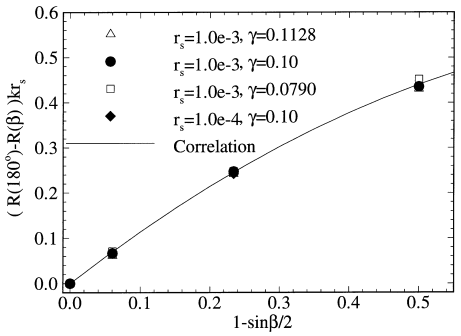

Fig. 9. Results showing the variation of the resistance for varying contact angles and the resulting correlation.

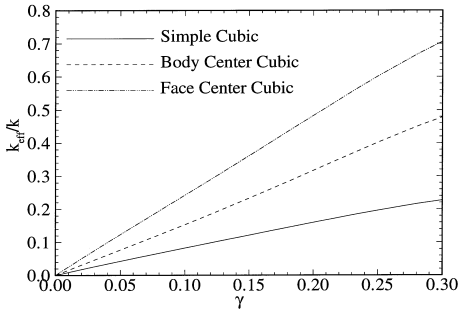

Fig. 10. Results showing the variation of the dimensionless conductivity for different unit cell configurations and contact radius ratios.

less conductivity varies linearly with the contact-area ratio, γ, and with a correlation coefficient of 0.99, the subsequent correlations are given below in Eqs. (14).

$$\text{SC:} \quad \frac{k_{\text{eff}}}{k} = 0.8278\gamma \tag{14a}$$

$$\text{BCC:} \quad \frac{k_{\text{eff}}}{k} = 1.5336\gamma \tag{14b}$$

$$\text{FCC:} \quad \frac{k_{\text{eff}}}{k} = 2.4211\gamma \tag{14c}$$

To assess the exact impact of the contact angle, β, the above calculations are repeated by substituting $R(\beta)$ in Eq. (6) with $R(180)$ from Eq. (13). The resulting values are then compared against those obtained above and the subsequent percentage error is computed for various contact radius ratio, γ. The results, shown in Fig. 11, indicate the error to be larger in calculating the conductivity for the BCC unit cell than for the FCC unit cell. This is due to the contact angle in the BCC cell to be further from 180° than the contact angle in the FCC unit cell. In addition, the error increases almost linearly with increasing contact radius

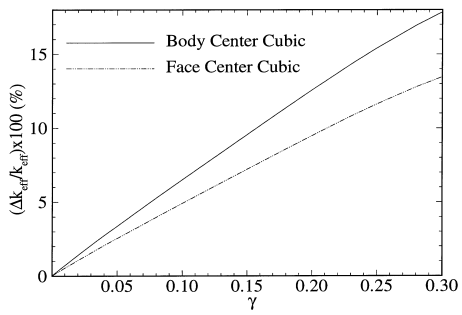

Fig. 11. Results showing the percentage error incurred in calculating the effective thermal conductivity of different unit cell without accounting for the effect of the contact angles.

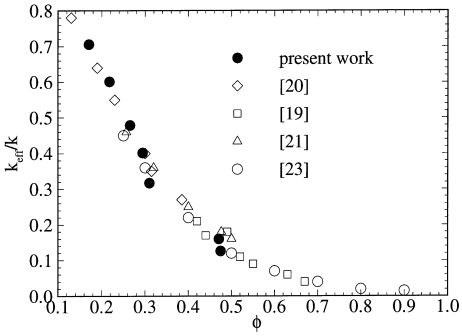

Fig. 12. Results showing excellent agreement between the currently computed effective conductivity and those obtained by previous investigators.

ratio, and with the present set of parameter, reaches a maximum value of 18%. Clearly, the effect of the contact angle cannot be neglected.

Finally, using the current model, the effective conductivity was computed for packed beds with seven different porosity values ranging from 0.18 to 0.47. For each packed bed, the porosity value was used to determine the appropriate unit cell (Table 1), and through Eq. (1) and Table 2 an appropriate value of the contact radius ratio was determined. Using this contact radius ratio and the chosen unit cell, the effective thermal conductivity was determined through Eq. (14). The results are then compared against previous experimental results from the powder sintering literature [19,20], and the heat transfer literature [21], as well as against the modeling results obtained from the physics literature [22]. As shown in Fig. 12, the agreement was excellent.

4. Conclusion

An alternative method is herein presented whereby packed beds are approximated as packed sphere systems consisting of the SC, BCC or FCC unit cells. The present method is valid for packed beds of porosity between 0.5 and 0.2, and where the conductivity of the sphere is much larger than that of the surrounding matrix. This method relies on first identifying the appropriate unit-cell configuration from the given porosity, and using such configuration to compute the effective thermal conductivity. This conductivity was computed through constriction resistance relations, which were presently computed and correlated. A finite volume scheme in conjunction with a MSTG method was utilized to compute the necessary relations. These results were correlated and presented. The results showed for the first time the necessity of accounting for the angles between the contacting spheres.

Accounting for this contact angle, the effective thermal conductivity was computed for packed beds of different porosities, and excellent agreement was obtained.

Acknowledgements

The authors would like to acknowledge the financial support from the Department of Mechanical Engineering at HKUST, and the following grant agencies of the Hong Kong SAR Government: The University Grant Council (Grant #DAG93/94.EG26, DAG98/99.EG21) and the Research Grant Council (Grant #HKUST807/96E).

References

[1] R.C. McPhedran, D.R. McKenzie, The conductivity of lattices of spheres: I. The simple cubic lattice, Proc. R. Soc. Lond. A 359 (1978) 45–63.
[2] D.R. Shonnard, S. Whitaker, The effective thermal conductivity for a point-contact porous medium; and experimental study, International Journal of Heat and Mass Transfer 32 (1989) 503–512.
[3] D. Veyret, S. Cioulachtjian, L. Tadrist, J. Pantaloni, Effective thermal conductivity of a composite material: a numerical approach, Journal of Heat Transfer 155 (1993) 866–871.
[4] G. Buonanno, A. Carotenuto, The effective thermal conductivity of a porous medium with interconnected particles, International Journal of Heat and Mass Transfer 40 (1997) 393–405.
[5] C.T. Hsu, K.W. Wong, P. Cheng, Effects of particle shape and configuration on the thermal conductivity of a porous medium, in: Proceedings of the Tenth International Heat Transfer Conference, Brighton, UK, vol. 6, 1994, pp. 367–372.
[6] S.-Y. Lu, Anisotropy in effective conductivities of rectangular arrays of elliptic cylinders, Journal of Applied Physics 76 (1994) 2641–2647.
[7] S. May, S. Tokarzewsk, A. Zaechara, B. Cichocki, Continued fraction representation for the effective thermal conductivity coefficient of a regular two-component composite, International Journal of Heat and Mass Transfer 37 (1994) 2165–2173.
[8] S. Tokarzewsk, J. Blawzdziewicz, I. Andrianov, Effective conductivity for densely packed highly conducting cylinders, Applied Physics A 59 (1994) 601–604.
[9] L.S. Verma, A.K. Shrotriya, R. Singh, D.R. Chaudhary, Thermal conduction in two-phase materials with spherical and non-spherical inclusions, Journal of Physics, D: Applied Physics 24 (1991) 1729–1737.
[10] J. Kallweit, E. Hahne, Effective thermal conductivity of metal hydride powder: measurement and theoretical modelling, in: Proceedings of the Tenth International Heat Transfer Conference, Brighton, UK, vol. 6, 1994, pp. 373–378.
[11] W.W.M. Siu, S.H.-K. Lee, Transient temperature computation for a system of multiple contacting spheres in 180° orientation, ASME Publication HTD-Vol. 339, 1997, pp. 151–160.
[12] E. Arzt, The influence of an increasing particle coordination in the densification of spherical powders, Acta Metallurgy 30 (1982) 1833–1890.
[13] R.M. German, Powder Metallurgy Science, 2nd ed., Metal Powder Industries Federation, NJ, 1994.
[14] C. Dellis, D. Bouvard, P. Stutz, Numerical modeling of particle deformation, in: Hot Isostatic Pressing'93, Elsevier Science, Amsterdam, 1994, pp. 53–60.
[15] J.V. Beck, J.R. Lloyd, Transient surface temperatures in solids due to small heat sources, Win Aung (Ed.), Cooling Technology for Electronic Equipment, Hemisphere, Washington, DC, 1988, pp. 465–483.
[16] K.J. Negus, M.M. Yovanovich, J.V. Beck, On the nondimensionalization of constriction resistance for semi-infinite heat flux tube, Journal of Heat Transfer 111 (1989) 804–807.
[17] W.W.M. Siu, S.H.-K. Lee, Multi-spatial-temporal grids for three-dimensional transient conduction problems, Numerical Heat Transfer — Part B 26 (1999) 163–181.
[18] Y. Jaluria, K.E. Torrance, Computational Heat Transfer, Hemisphere, New York, 1986.
[19] J.C.Y. Koh, E.P. Casal, R.W. del Evans, V. Derlugin, Fluid flow and heat transfer in high temperature porous matrices for transpiration cooling, AFFDL-TR-66–70, 1966.
[20] J.C.Y. Koh, A. Fortini, Thermal conductivity and electrical resistivity of porous material NASA CR-120854, 1971.
[21] J.S. Agapiou, M.F. DeVries, An experimental determination of the thermal conductivity of a 304L stainless steel powder metallurgy material, Journal of Heat Transfer 111 (1989) 281–286.
[22] S. Torquato, I.C. Kim, D. Cule, Effective conductivity, dielectric constant, and diffusion coefficient of digitized composite media via first-passage-time equations, Journal of Applied Physics 85 (1999) 1471–1560.
[23] M.G. Kaganer, Contact heat transfer in granular material under vacuum, Journal of Engineering Physics 11 (1966) 19–22.
[24] C. Argento, D. Bouvard, Modeling the effective thermal conductivity of random packing of spheres through densification, International Journal of Heat and Mass Transfer 39 (1996) 1343–1350.